

**PHOTONIC CRYSTAL WAVEGUIDES:  
A ONE-DIMENSIONAL MODEL THEORY**

**Brian Stout**

Institut Fresnel, Unité Mixte de Recherche du Centre National de la  
Recherche Scientifique n° 6133, Faculté des Sciences et Techniques, Centre de  
Saint

Jérôme, 13397 Marseille Cedex 20, France  
brian.stout@fresnel.fr

**Sophie Stout**

Case 46, Université de Provence  
3 Place Victor Hugo 1331, Marseille Cedex 3, France  
sophie.stout@photons.u-3mrs.fr

**Michel Nevière**

Institut Fresnel, Unité Mixte de Recherche du Centre National de la  
Recherche Scientifique n° 6133, Faculté des Sciences et Techniques, Centre de  
Saint

Jérôme, 13397 Marseille Cedex 20, France

**Abstract**– We study the dispersion relations and field maps of the propagating modes in one dimensional models of photonic crystal fibers. This simple model allows the derivation of rigorous electromagnetic theory, and provides insight for the properties observed in actual waveguides. The theory is developed through a particularly efficient impedance formulation of the problem. The dispersion relations of propagating modes are presented and discussed. Field maps of certain modes are also illustrated, and allow an understanding of the low loss behavior of photonic fibers.

---

**Contents**

<b>1. Model of a photonic crystal waveguide in 1-dimension.</b>	963
1.1. Field configurations and notations	964
1.2. Impedance Formulation	968
<b>2. Photonic waveguide design</b>	969
2.1. Attenuation in a finite crystal	973
2.2. Field map	976
2.3. Dispersion relations	979
2.4. Absorption in photonic crystal fibers	984
<b>3. Conclusion</b>	986
<b>References</b>	987

There is a considerable interest in photonic crystal waveguides, also known as “holey fibers”, or PBF (Photonic Band-gap Fibers).[1–5] Due to structural complexity of such fibers, theoretical simulations can play an important role in predicting their design and mode characteristics. Although realistic two-dimensional simulations of such fibers are possible using current techniques and computers,[6] numerically exact 2-D calculations are both unwieldy and time-consuming. In the study of such waveguides, it may therefore prove useful to perform exact calculations in a simpler 1-D system exhibiting similar behavior. In this work we present and study such a 1-D model of PBFs. Despite this simplification, the problem still presents considerable numerical difficulties and requires particularly efficient and reliable theoretical techniques. Calculations in the 1-D system prove particularly interesting in the study of dispersion relations where calculations for a large number of frequencies are necessary.

We shall particularly look at TE modes in PBFs having a low index core for which the light is guided purely by the photonic band-gap effect.[7, 8] In section (1), we describe the model, and the analytical impedance techniques employed to determine the propagative modes. Our method formulates the scattering in terms of entry impedances in a technique analogous to network theory. This type of technique was first developed in the context of diffraction gratings with multiple coating layers,[9]. In section (2.2.1), we derive formulae for estimating the attenuation in a PBF due to transmission through the photonic crystallin walls (assuming zero absorption). The validity of the absorption free assumption will be tested in section (2.2.4) by adding absorption to the high index material. We will see that a fiber alternating between a high index and vacuum can have small absorption since most of the field is located in the absorption-free

vacuum. This result thus recommends vacuum filled PBFs as a means of guiding high intensity laser light since the influence of losses in silica will have smaller influence. Also, nonlinear effects which distort laser pulses will be reduced. TM modes, as well as other types of PBFs and their applications will be considered in a future publication.

### 1. MODEL OF A PHOTONIC CRYSTAL WAVEGUIDE IN 1-DIMENSION.

The model of a 1-dimensional slab gives a great deal of insight into the behavior of ordinary optical waveguides. One of the principal advantages of this model is that TE and TM waves decouple, and can therefore be treated separately. In this work, we model exclusively PBFs which guide TE waves entirely by the photonic band-gap effect. Specifically, we model fibers in which the light is to be “trapped” by the photonic crystal in a low index “defect” cavity in the center of the fiber (see fig.1).

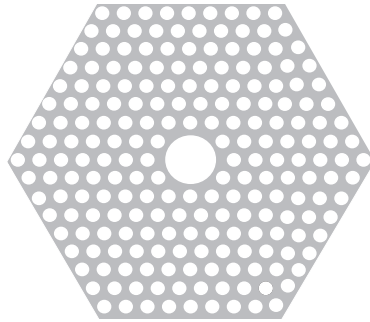


Fig. 1

FIG. 1: Schematic cross section of a photonic band-gap fiber. Low index “holes” are in white, while the high index material is gray. Light is to be guided in the large central “defect” hole by the surrounding photonic crystal

In this work, we adopt a 1-dimensional model of PBFs (fig.2), where the 2-D photonic crystal is replaced by  $\mathcal{N}$  bi-layer slabs, each bi-layer slab consisting

of a slab of a high index material,  $n_h$  and a slab of a low index “background” layer,  $n_b$ . These two Bragg type stacks surround a central layer of index  $n_c$ . All these refractive indices need not be entirely real, and may have imaginary parts to take into account the absorption present in actual materials. In view of this as a model for a 2-D system, we assume that the superstrate and substrate are composed of identical materials of (real) refractive index  $n_1$ . This model is then very similar to a Bragg mirror Fabry-Perot interferometer. Nevertheless, in our model, we are not interested in the presence of transmission peaks, but in the precise properties of a “leaky” wave guided in the central low index gap.

We adopt an impedance formulation of the multilayer problem which can be manipulated to yield the precise values of the propagation constant necessary for guided mode calculations. To a certain approximation, this method yields analytical formulas which may prove useful in preliminary fiber design and a qualitative understanding of mode characteristics.

Let us look at the 1-D model of a low index core PBF in detail (fig.2). The model consists of  $N$  planar interfaces separating  $N + 1$  regions (labeled by the index  $j$ ); the superstrate is labeled region 1, and the substrate region  $N + 1$ . The direction of the propagation of the mode is labeled  $\hat{\mathbf{x}}$ , and the direction normal to the interfaces  $\hat{\mathbf{y}}$ . The low index layer of the innermost bi-layer is excluded in this model, thus allowing us to conveniently consider the situation where the core material is identical to the low index material ( $n_c = n_b$ ). With these specifications, there are  $N = 4\mathcal{N}$  interfaces in this system (we recall that  $\mathcal{N}$  is the number of high index layers on each side of the “defect” layer).

The objective is to determine the optimal fiber design, and to calculate the characteristics of the modes of propagation. We choose to formulate these solutions within the context of a scattering formulation. Namely, we will calculate the reflection and transmission coefficients from a 1-dimensional stratified medium. As detailed below, the propagation constant of a mode corresponds to a pole in the reflection and transmission coefficients.

### 1.1. Field configurations and notations

The electric field is studied in the time-harmonic regime

$$\mathbf{E}(t, \mathbf{r}) = \text{Re} [\mathcal{E}(\mathbf{r})e^{-i\omega t}]. \quad (1)$$

The electromagnetic equations for a medium in which the constitutive parameters,  $\varepsilon$  and  $\mu$  vary only in the  $\hat{\mathbf{y}}$  direction is

$$\nabla \times \mu^{-1}(y)\nabla \times \mathcal{E}(\mathbf{r}) - \omega^2 \varepsilon(y) \mathcal{E}(\mathbf{r}) = 0 \quad (2)$$

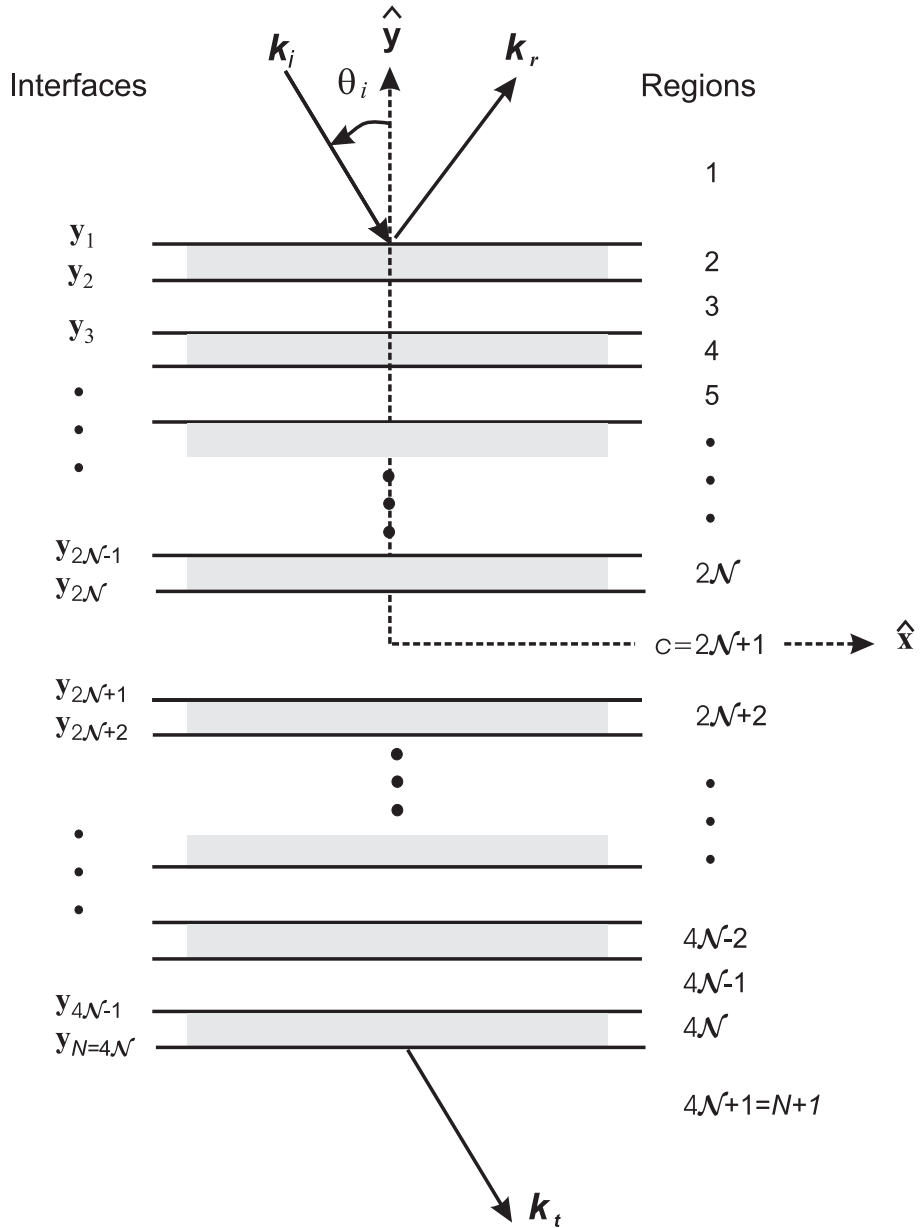


Fig. 2

FIG. 2: One-dimensional model of a photonic band-gap fiber. A central low index slab;  $j = 2\mathcal{N}+1$ , surrounded by 1-D photonic crystal stacks composed of  $\mathcal{N}$  high index layers. The  $\hat{y}$  direction is perpendicular to the slab interfaces while  $\hat{x}$  is in the direction of propagation. There are  $N = 4\mathcal{N}$  interfaces, and the substrate and superstrate are composed of identical materials. In the scattering formalism, one considers a downward propagating incident wave, and consequent reflected and transmitted waves

An incident plane wave is taken to be a downward propagating wave with a wavevector  $\mathbf{k}_1$  at an angle  $\theta_1$  with respect to the normal of the interfaces (see fig.2).

For slabs whose constitutive parameters are piecewise constant, the solution is obtained by considering linear superpositions of ascending and descending waves within each layer, and adjusting the coefficients so as to satisfy the boundary conditions. Solutions to the Maxwell equations for TE waves within each homogenous slab susceptible to satisfy the boundary conditions are written

$$\mathcal{E}^{(j)}(\mathbf{r}) = u_j(x, y)\mathbf{e}_z \quad (3)$$

where  $\mathbf{e}_z$  is a unit vector pointing in the  $\hat{\mathbf{z}}$  direction, and the  $u_j(x, y)$  are of the form

$$u_j(x, y) = (a_j^- e^{-i\beta_j y} + a_j^+ e^{i\beta_j y}) e^{i\gamma x}. \quad (4)$$

where  $a_j^+$  and  $a_j^-$  are respectively the coefficients of the ascending and descending waves. The constants  $\gamma$  and  $\beta_j$  are expressed

$$\begin{aligned} \gamma &\equiv k_1 \sin \theta_1 \\ \beta_j &\equiv \sqrt{k_j^2 - \gamma^2} \end{aligned} \quad (5)$$

where the wave numbers  $k_j$  satisfy the homogenous dispersion relations

$$k_j^2 = \varepsilon_j \mu_j \left(\frac{\omega}{c}\right)^2 \quad (6)$$

with  $\varepsilon_j$  and  $\mu_j$  denoting the relative primitivities.

We formulate the problem in the context of reflection-transmission. That is, we construct field solutions resulting from a downward moving incident plane wave with amplitude  $a_1^-$ , and for which there is only a downward component,  $a_{N+1}^-$ , in the substrate ( $a_{N+1}^+ \equiv 0$ ). The amplitude of the upward-going wave in the superstrate,  $a_1^+$ , corresponds to the reflected wave. The reflection and transmission coefficients for the amplitudes are defined respectively as the ratio, with respect to the incident wave amplitude of the upward and downward going wave amplitudes in the superstrate and substrate :

$$r \equiv \frac{a_1^+}{a_1^-} \quad t \equiv \frac{a_{N+1}^-}{a_1^-}. \quad (7)$$

We adopt the definition of a propagative mode as a non-trivial solution ( $a_{N+1}^-$  and  $a_1^+$  both  $\neq 0$ ) of the electromagnetic equations in the absence of an incident wave, *i.e.* for which  $a_1^- = 0$  (solution of the homogenous boundary value

problem). With this definition, a mode corresponds to a solution for which both  $r$  and  $t$  tend to infinity. The solution of the problem is then to determine the field coefficients in each slab, eq.(4), which satisfy the boundary conditions at the slab interfaces, and also satisfy the condition for the existence of a mode, ( $a_1^- = a_{N+1}^+ = 0$ ).

In this work,  $\bar{n}_j$  is defined as the refraction index “normalized” with respect to material 1 :

$$\bar{n}_j \equiv \frac{k_j}{k_1} = \frac{n_j}{n_1} = \sqrt{\frac{\epsilon_j \mu_j}{\epsilon_1 \mu_1}}. \tag{8}$$

It is also convenient to adopt dimensionless parameters for describing the field characteristics :

$$\delta \equiv \frac{\gamma}{k_1} = \sin \theta_1 \tag{9}$$

and

$$\alpha_j \equiv \sqrt{\bar{n}_j^2 - \delta^2} = \frac{\beta_j}{k_1}. \tag{10}$$

Due to the fact that the square root is a multi-valued function, we must determine branch cuts in the complex plane in order to select the physical solutions. Employing this technique, developed in ref.[10], the branch cuts may be chosen such that the physical solutions are those which satisfy

$$\text{Re} \{ \alpha_j \} + \text{Im} \{ \alpha_j \} > 0. \tag{11}$$

It is sometimes useful conceptually to describe  $\alpha_j$  and  $\delta$  in terms of an “angle” of propagation,  $\theta_j$ , within each layer

$$\begin{aligned} \alpha_j &\equiv \frac{1}{k_1} \sqrt{k_j^2 - \gamma^2} \\ &= \frac{k_j}{k_1} \sqrt{1 - \left( \frac{\delta}{\bar{n}_j} \right)^2} \\ &\equiv \frac{k_j}{k_1} \cos \theta_j \\ \frac{\delta}{\bar{n}_j} &\equiv \sin \theta_j \end{aligned} \tag{12}$$

Although this definition satisfies the relation  $\sin^2 \theta_j + \cos^2 \theta_j = 1$ , it is important to remark that  $\theta_j$  is not necessarily real. Notably, the angle  $\theta_j$  will be complex, should  $\bar{n}_j$  or  $\delta$  be complex. A complex  $\bar{n}_j$  corresponds to absorption or diffusion within the slabs.

### 1.2. Impedance Formulation

A number of techniques exist in the literature. Many of these techniques encounter numerical instabilities, particularly in the case of absorbing media. Even for techniques which are numerically stable (such as the  $S$ -matrix propagation formalism), the closeness of  $\delta$  to the real axis generally makes it quite difficult to determine its imaginary component precisely. In this paragraph, we give the principal results of an impedance method which, in the 1-D model, will permit the determination of  $\delta$  in an efficient manner.

The impedances of the materials of different slabs are expressed as :

$$z_j \equiv \sqrt{\frac{\mu_j \mu_0}{\varepsilon_j \varepsilon_0}} \quad (13)$$

where  $\varepsilon_0$  and  $\mu_0$  are the constitutive constants of the vacuum; we define a dimensionless "region" impedance,  $Z_j$ , for TE waves by the formula :

$$\begin{aligned} Z_j &\equiv \frac{\mu_j}{\mu_1} \frac{1}{\alpha_j} & j \in [1, N+1] & \quad (14) \\ &= \sqrt{\frac{\mu_j \varepsilon_1}{\varepsilon_j \mu_1}} \frac{1}{\cos \theta_j} = \frac{z_j}{z_1} \frac{1}{\cos \theta_j}. \end{aligned}$$

We note that since the electric field is polarized perpendicular to the plane of incidence, the magnetic field lies in the plane of incidence. Of the two components of the magnetic field, only the  $\mathcal{H}_x$  component is tangential to the boundary layer. The dimensionless *entry* impedance of the  $j^{\text{th}}$  interface,  $Z_{\text{en}}^{(j)}$ , for a TE wave is then defined via the ratio of the tangential field components evaluated at the  $j^{\text{th}}$  interface

$$Z_{\text{en}}^{(j)} \equiv \frac{1}{z_1} \left. \frac{\mathcal{E}_z^{(j)}}{\mathcal{H}_x^{(j)}} \right|_{y=y_j} = \frac{1}{z_1} \left. \frac{\mathcal{E}_z^{(j+1)}}{\mathcal{H}_x^{(j+1)}} \right|_{y=y_j} \quad j \in [1, N] \quad (15)$$

where the  $z_1$  factor serves to make  $Z_{\text{en}}^{(j)}$  a dimensionless quantity by normalizing it with respect to the impedance of the superstrate. The boundary conditions impose that the entry impedance must be continuous across the boundary layers. After some algebra, the continuity of the entry impedance at the interfaces can be reformulated in terms of a recurrence relation for entry impedances in formulae analogous to those of network theory

$$Z_{\text{en}}^{(j-1)} = Z_j \frac{Z_{\text{en}}^{(j)} - Z_j i \tan \psi_j}{Z_j - Z_{\text{en}}^{(j)} i \tan \psi_j} \quad j \in [2, N] \quad (16)$$

where the  $\psi_j$  are defined

$$\psi_j \equiv \alpha_j (\bar{y}_j - \bar{y}_{j-1}) \quad j \in [2, N]. \quad (17)$$

The  $\bar{y}_j$  are the dimensionless  $y$  coordinates of the interfaces

$$\bar{y}_j \equiv y_j k_1 \quad j \in [1, N] \quad (18)$$

The initial value for the recurrence relation is determined by the entry impedance evaluated on the lower part of the interface with the substrate

$$Z_{\text{en}}^{(N)} = \frac{1}{z_1} \left. \frac{\mathcal{E}_z^{(N+1)}}{\mathcal{H}_x^{(N+1)}} \right|_{y=y_N} = -Z_{N+1} \quad (19)$$

It will also prove useful to rewrite the upward recurrence relation, eq.(16), as a downward recurrence relation :

$$Z_{\text{en}}^{(j)} = Z^{(j)} \frac{Z_{\text{en}}^{(j-1)} + Z^{(j)} i \tan \psi_j}{Z^{(j)} + Z_{\text{en}}^{(j-1)} i \tan \psi_j} \quad j \in [2, N] \quad (20)$$

The impedance formulation yields a rather simple expression for the reflection coefficient :

$$r = \frac{Z_1 + Z_{\text{en}}^{(1)}}{Z_{\text{en}}^{(1)} - Z_1} e^{-2i\alpha_1 \bar{y}_1} \quad (21)$$

The expression for the transmission coefficient is considerably more complex. Nevertheless, we show in section (2.2.2) that it may be expressed as :

$$t = -2 \frac{Z_{N+1}}{Z_{\text{en}}^{(1)} - Z_1} \tau_j \quad (22)$$

where  $\tau_j$  is a factor determined from a recurrence relation. We recall that we defined propagative modes as solutions to the scattering problem for which  $r$  and  $t$  both diverge. We readily deduce from eqs.(21)-(22) that propagative modes occur when

$$Z_{\text{en}}^{(1)} = Z_1. \quad (23)$$

## 2. PHOTONIC WAVEGUIDE DESIGN

There are many opto-geometrical parameters to characterize a photonic crystal waveguide (thickness of the external layers, number of layers, thickness of

the central layer, etc.). In order to simplify this specification, we choose the layer thicknesses such that they “optimize” a PBF waveguide with crystalline walls of infinite order and lossless dielectric constants. In subsequent paragraphs, these “optimal” values for the layer thicknesses will be adopted when treating waveguides with a finite number of layers which are composed of low loss dielectrics.

Specifically, we choose the multi-layer stacks surrounding the central air gap (fig.2) to have Bragg type parameters for a frequency  $\omega_{\text{op}}$ , and for a (real) incidence angle characterized by  $\delta_{\text{op}} = \sin \theta_{\text{op}}$ . It is often convenient to replace  $\omega_{\text{op}}$  by the wavelength in the external medium at the optimal frequency,  $\lambda_1^{\text{op}} \equiv \frac{2\pi c}{n_1 \omega_{\text{op}}}$ . Having chosen the properties of the cladding, the thickness of the central layer will be chosen such that there exists a mode of propagation of order,  $m_{\text{op}}$ . As we will see below, the specification  $(\delta_{\text{op}}, \omega_{\text{op}}, m_{\text{op}})$  and the constitutive parameters of the layers suffice to determine the thicknesses of all layers.

Assuming minimal layer thicknesses, and real refractive indexes, the usual Bragg mirror parameters are obtained by imposing for the cladding layers, that

$$\psi_j \equiv \alpha_j (\bar{y}_j - \bar{y}_{j-1}) \equiv \sqrt{\bar{n}_j^2 - \delta_{\text{op}}^2} \frac{2\pi}{\lambda_1^{\text{op}}} (y_j - y_{j-1}) = -\frac{\pi}{2} \quad \forall j \in [2, N], \quad j \neq 2N + 1 \quad (24)$$

From this relation, one finds that the thicknesses of the high and low index layers,  $\Delta y_h$  and  $\Delta y_b$  respectively, are :

$$\Delta y_h = \frac{1}{\sqrt{\bar{n}_h^2 - \delta_{\text{op}}^2}} \frac{\lambda_1^{\text{op}}}{4} = \frac{\lambda_h^{\text{op}}}{4 \cos \theta_h} \quad (25)$$

$$\Delta y_b = \frac{1}{\sqrt{\bar{n}_b^2 - \delta_{\text{op}}^2}} \frac{\lambda_1^{\text{op}}}{4} = \frac{\lambda_b^{\text{op}}}{4 \cos \theta_b} \quad (26)$$

where  $\lambda_h^{\text{op}} \equiv \lambda_1^{\text{op}} / \bar{n}_h$  and  $\lambda_b^{\text{op}} \equiv \lambda_1^{\text{op}} / \bar{n}_b$  are the wavelengths in the high and low index media respectively. As we will see below, this choice of layer thicknesses is particularly useful due to the fact that  $|\tan \psi_{h,b}| \rightarrow \infty$  for all cladding layers. We will see below that this property greatly simplifies the recurrence relations and permits analytic evaluations of the modes at this point. From these formulae, we observe that the filling fraction of the high index material,  $f_h$ , is a function of  $\delta_{\text{op}}$  and given by the formula :

$$f_h \equiv \frac{\Delta y_h}{\Delta y_b + \Delta y_h} = \frac{\sqrt{\bar{n}_b^2 - \delta_{\text{op}}^2}}{\sqrt{\bar{n}_b^2 - \delta_{\text{op}}^2} + \sqrt{\bar{n}_h^2 - \delta_{\text{op}}^2}} \quad (27)$$

Typical values of the filling fraction are given in fig.3 for refractive indices  $n_h = 1.95$ , and  $n_b = n_1 = 1$ .

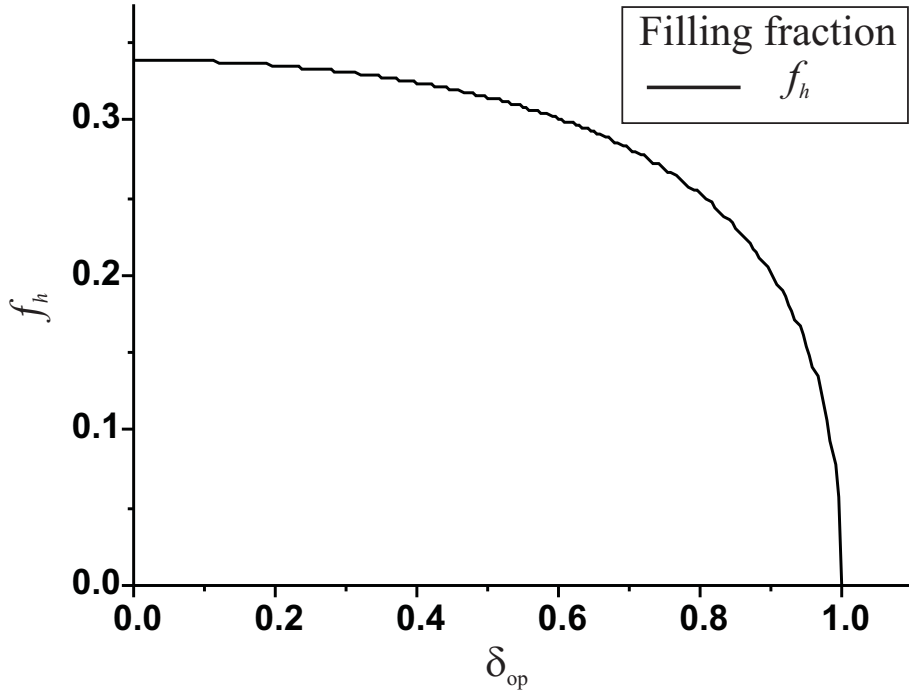


FIG. 3: Filling fraction of the high index material as a function of the design parameter  $\delta_{\text{op}}$ . The index of the high and low index materials are taken as  $\bar{n}_h = 1.95$  and  $\bar{n}_b = \bar{n}_c = 1$  respectively.

Having fixed the design properties of the multi-layers for a given  $(\omega_{\text{op}}, \delta_{\text{op}})$ , we can determine a thickness of the central region for which the  $(\omega_{\text{op}}, \delta_{\text{op}})$  pair describes a mode in the infinite crystal limit. Recalling that the thicknesses of the photonic crystal layers were chosen such that  $|\tan \psi_{h,b}| \rightarrow \infty$ , the upward-going recursion formula for the entry impedances, eq.(16), greatly simplifies to

$$Z_{\text{en}}^{(j-1)} = \frac{Z_j^2}{Z_{\text{en}}^{(j)}} \quad (28)$$

with an initial value of

$$Z_{\text{en}}^{(N)} = -Z_{N+1} = -Z_1. \quad (29)$$

Invoking this relation up to the interface just below the central air layer, we

obtain

$$Z_{\text{en}}^{(2\mathcal{N}+1)} = -\frac{Z_h^{2\mathcal{N}}}{Z_1 Z_b^{2\mathcal{N}-2}} = -\frac{Z_b^2}{Z_1} \left(\frac{Z_h}{Z_b}\right)^{2\mathcal{N}}. \quad (30)$$

The physical significance of this result lies in the fact the condition  $n_h > n_b$  implies that  $\left|\frac{Z_h}{Z_b}\right| < 1$  and consequently, eq.(21), tells us that the reflectivity coefficient of this stack inside the central layer is  $r = \frac{Z_1 + Z_{\text{en}}^{(2\mathcal{N}+1)}}{Z_{\text{en}}^{(2\mathcal{N}+1)} - Z_1} e^{-2i\alpha_c \bar{y}_{2\mathcal{N}+1}}$  from we deduce  $|r| = 1$  in the infinite crystal limit, *i.e.*  $\mathcal{N} \rightarrow \infty$ . We thus conclude that the infinite lower stack is a perfect reflector as desired.

Continuing the recurrence relation up to the uppermost interface of the stack, we saw in section (1.1.2) that the condition for the existence of a mode is :

$$Z_{\text{en}}^{(1)} = Z_1 \quad (31)$$

Applying this condition as a starting value, and applying the recurrence relation, eq.(28), backwards for the same thicknesses as above, *i.e.* eqs.(25), (26) one finds :

$$Z_{\text{en}}^{(j)} = \frac{Z_j^2}{Z_{\text{en}}^{(j-1)}}. \quad (32)$$

The application of this recurrence allows us to conclude that the condition for a propagating mode is that the entry impedance at interface just above the central layer is

$$Z_{\text{en}}^{(2\mathcal{N})} = \frac{Z_h^{2\mathcal{N}}}{Z_1 Z_b^{2\mathcal{N}-2}} = \frac{Z_b^2}{Z_1} \left(\frac{Z_h}{Z_b}\right)^{2\mathcal{N}}. \quad (33)$$

In order for eq.(30) and eq.(33) to be consistent, the upward recurrence relation, eq.(16), must be verified for the interfaces  $2\mathcal{N}$  and  $2\mathcal{N} + 1$ . This condition can be rewritten

$$\begin{aligned} \tan \psi_{2\mathcal{N}+1} &= iZ_c \frac{Z_{\text{en}}^{(2\mathcal{N})} - Z_{\text{en}}^{(2\mathcal{N}+1)}}{Z_c^2 - Z_{\text{en}}^{(2\mathcal{N})} Z_{\text{en}}^{(2\mathcal{N}+1)}} \\ &= 2iZ_c \frac{\frac{Z_b^{2\mathcal{N}}}{Z_1 Z_b^{2\mathcal{N}-2}}}{Z_c^2 + \left[\frac{Z_b^{2\mathcal{N}}}{Z_1 Z_b^{2\mathcal{N}-2}}\right]^2} \\ &\equiv i\phi \end{aligned} \quad (34)$$

where in the second line we have inserted the conditions of eq.(30) and eq.(33). From the fact that  $\left|\frac{Z_h}{Z_b}\right| < 1$ , we deduce that, in the limit of  $\mathcal{N} \rightarrow \infty$ ,

$\tan \psi_{2\mathcal{N}+1} = 0$ . The solutions are then

$$\psi_{2\mathcal{N}+1} = -m_{\text{op}}\pi \quad m_{\text{op}} = 1, 2, \dots \quad (35)$$

where  $m_{\text{op}}$  numbers the optimum modes of the solution. The central gap thickness,  $\Delta y_c$ , is then derived from

$$\psi_c \equiv \psi_{2\mathcal{N}+1} \equiv \alpha_{2\mathcal{N}+1} (\bar{y}_{2\mathcal{N}+1} - \bar{y}_{2\mathcal{N}}) = -k_1^{\text{op}} \Delta y_c \sqrt{\bar{n}_c^2 - \delta_{\text{op}}^2} = -m_{\text{op}}\pi$$

$$m_{\text{op}} = 1, 2, \dots \quad (36)$$

*i.e.*

$$\Delta y_c = \frac{m_{\text{op}}}{\sqrt{\bar{n}_c^2 - \delta_{\text{op}}^2}} \frac{\lambda_1^{\text{op}}}{2} \quad m_{\text{op}} = 1, 2, \dots \quad (37)$$

which is familiar as the condition for obtaining a transmission peak in a Fabry-Perot interferometer. One should remark that this is an exact solution in the infinite crystal limit, and that the propagation of the mode is described by purely real parameters frequency,  $\omega_{\text{op}}$  and propagation constant,  $\gamma = k_1^{\text{op}} \delta_{\text{op}}$ . These parameters are real because there is no loss through the infinite lossless photonic crystal. In the next section we look at the attenuation resulting from the presence of a finite crystal.

### 2.1. Attenuation in a finite crystal

One can now obtain approximate results for the attenuation of a finite crystal stack using the parameters chosen for an infinite stack. Let us continue to take  $Z_b$ ,  $Z_h$  and  $Z_c$  to be real numbers as a first approximation. Consequently, eq.(34) demands for a finite stack, that  $\tan \psi_c$  be a (small) pure imaginary number. The solutions to this equation are

$$\psi_c \simeq -m_{\text{op}}\pi + i\phi \quad m_{\text{op}} = 1, 2, \dots \quad (38)$$

From the definition of  $\psi_c$ , eq.(17), a complex value for this parameter can only be obtained by letting  $\omega$  or  $\delta$  be complex. It is common to call “leaky mode” a mode occurring (via analytic continuation) for complex  $\delta$ . We let  $\delta$  become complex,  $\delta \simeq \delta_{\text{op}} + i\delta''$ , and the central phase factor,  $\psi_c$ , corresponding to the

solution eq.(36), is then

$$\begin{aligned} \psi_c &\equiv -k_1 \Delta y_c \sqrt{\bar{n}_c^2 - (\delta_{op} + i\delta'')^2} \\ &\simeq -k_1 \Delta y_c \sqrt{\bar{n}_c^2 - \delta_{op}^2} \sqrt{1 - 2i \frac{\delta_{op} \delta''}{\bar{n}_c^2 - \delta_{op}^2}} \\ &\simeq -k_1 \Delta y_c \sqrt{\bar{n}_c^2 - \delta_{op}^2} \left( 1 - i \frac{\delta_{op} \delta''}{\bar{n}_c^2 - \delta_{op}^2} \right) \\ &= -m_{op} \pi + i m_{op} \pi \frac{\delta_{op} \delta''}{\bar{n}_c^2 - \delta_{op}^2} \end{aligned} \tag{39}$$

where we have made the reasonable approximation that  $\delta_{op} \delta'' \ll \bar{n}_c^2 - (\delta_{op})^2$ . Using the approximation  $\tan(-m_{op} \pi + i\eta) \simeq i\eta$  for integer  $m_{op}$ , and  $\eta \ll 1$ , comparison of eq.(34) and eq.(39) yields for the attenuation  $\delta''$

$$\delta'' \simeq 2Z_c \left( \frac{\bar{n}_c^2 - \delta_{op}^2}{m_{op} \pi \delta_{op}} \right) \frac{\frac{Z_h^{2N}}{Z_1 Z_b^{2N-2}}}{Z_c^2 + \left[ \frac{Z_h^{2N}}{Z_1 Z_b^{2N-2}} \right]^2} \quad m_{op} = 1, 2, \dots \tag{40}$$

For non magnetic media,  $\mu_j = \mu_1 \quad \forall j$ , and the region impedances simplify to

$$Z_j \equiv \frac{1}{\alpha_j} = \frac{1}{\sqrt{\bar{n}_j^2 - \delta^2}} \tag{41}$$

In this case, the formula for the attenuation simplifies to

$$\begin{aligned} \delta'' &\simeq \frac{2}{Z_c^2} \left( \frac{\bar{n}_c^2 - \delta_{op}^2}{\pi m_{op} \delta_{op}} \right) \frac{\frac{Z_c}{Z_1} \left( \frac{1}{\bar{n}_b^2 - \delta^2} \right) \left( \frac{\bar{n}_b^2 - \delta^2}{\bar{n}_h^2 - \delta^2} \right)^{\mathcal{N}}}{1 + \frac{1}{Z_c^2 Z_1^2} \frac{1}{(\bar{n}_b^2 - \delta^2)^2} \left( \frac{\bar{n}_b^2 - \delta^2}{\bar{n}_h^2 - \delta^2} \right)^{2\mathcal{N}}} \\ &= 2 \frac{(\bar{n}_c^2 - \delta_{op}^2)^2}{\pi m_{op} \delta_{op}} \frac{\frac{Z_c}{Z_1} \left( \frac{1}{\bar{n}_b^2 - \delta^2} \right) \left( \frac{\bar{n}_b^2 - \delta^2}{\bar{n}_h^2 - \delta^2} \right)^{\mathcal{N}}}{1 + \frac{(\bar{n}_c^2 - \delta^2)(1 - \delta^2)}{(\bar{n}_b^2 - \delta^2)^2} \left( \frac{\bar{n}_b^2 - \delta^2}{\bar{n}_h^2 - \delta^2} \right)^{2\mathcal{N}}} \end{aligned} \tag{42}$$

This formula simplifies even further if we remark that the low index layers, and central layer are all composed of the same absorption free material as the external medium, *i.e.*  $\bar{n}_b = \bar{n}_c = n_1 = 1$  (vacuum filled fibers placed in a vacuum for instance) :

$$\delta'' \simeq 2 \frac{(1 - \delta_{op}^2)^2}{m_{op} \pi \delta_{op}} \frac{1}{1 - \delta^2} \frac{\left( \frac{1 - \delta^2}{\bar{n}_h^2 - \delta^2} \right)^{\mathcal{N}}}{1 + \left( \frac{1 - \delta^2}{\bar{n}_h^2 - \delta^2} \right)^{2\mathcal{N}}} \tag{43}$$

For the small  $\delta''$  in which we are interested, the  $\left(\frac{1-(\delta')^2}{\bar{n}_h^2-(\delta')^2}\right)^{2\mathcal{N}}$  term in the denominator is completely negligible, and to a good approximation

$$\begin{aligned} \delta'' &\simeq 2 \frac{(1 - \delta_{\text{op}}^2)^2 (1 - \delta^2)^{\mathcal{N}-1}}{m_{\text{op}} \pi \delta_{\text{op}} (\bar{n}_h^2 - \delta^2)^{\mathcal{N}}} \\ &\simeq 2 \frac{(1 - \delta_{\text{op}}^2) (1 - \delta_{\text{op}}^2)^{\mathcal{N}}}{m_{\text{op}} \pi \delta_{\text{op}} (\bar{n}_h^2 - \delta_{\text{op}}^2)^{\mathcal{N}}} \end{aligned} \tag{44}$$

This formula is only approximate, since once that we allow  $\delta''$  to be non-zero, we no longer have  $\tan \psi_j = -\frac{\pi}{2}$  in the layers, and the simplified recursion relations used in deriving eq.(44) are no longer exact. Although it is possible to calculate the corrections to this formula, the simplest procedure at this point is to employ the technique described in section (2.2.3) for determining the  $\delta$  of the propagating modes for arbitrary frequencies. In figure 4, we plot, on a logarithmic scale, the attenuation  $\delta''$  for the fiber modes propagating at  $\omega_{\text{op}}$  in a fiber designed to propagate the lowest mode,  $m_{\text{op}} = 1$ , as a function of  $\delta_{\text{op}}$  for different  $\mathcal{N}$ . The physical parameters were taken as the vacuum for the core and low index material,  $\bar{n}_b = \bar{n}_c = 1$ , alternating with a high index dielectric  $\bar{n}_h = 1.95$ .

It is interesting to compare this attenuation with that obtained for current fiber optic technology which allows the fabrication of optical waveguides having extremely low losses (descending down to the order of 0.15 db/km). This implies that a signal starting with  $I_0$  intensity will have after one kilometer of travel, an intensity  $I$  given by

$$\begin{aligned} 10 \log_{10} \frac{I_0}{I} &= 0.15 \\ I &\simeq 0,966 I_0 \end{aligned}$$

This loss can arise from both imperfections in the fiber which induce scattering outside of the fiber, and by absorption of electromagnetic energy by the fiber material. Considering the Poynting theorem for an ordinary waveguide, we obtain that the attenuation in the  $x$  direction is expressed

$$\frac{I}{I_0} = e^{-2x \text{Im } \gamma} = e^{-2x k_1 \text{Im } \delta} \tag{45}$$

which gives an expression for  $\text{Im } \delta$  of

$$\text{Im } \delta = -\frac{\lambda_1}{4\pi x} \ln \frac{I}{I_0} \tag{46}$$

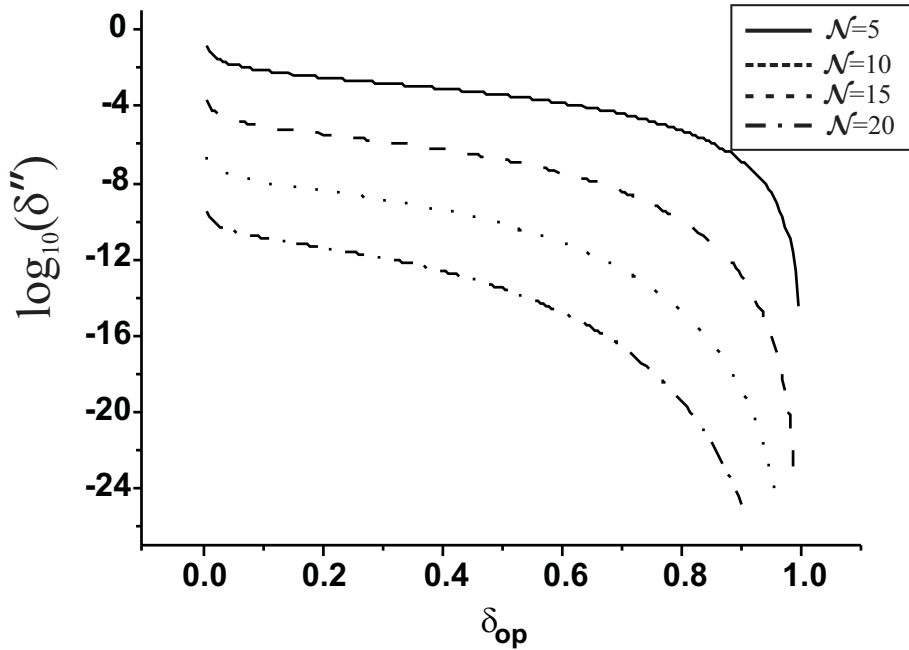


FIG. 4: Attenuation  $\delta''$  in finite 1-D fibers operating at frequency  $\omega_{\text{op}}$ , plotted as a function of  $\delta_{\text{op}}$  for different values of  $\mathcal{N}$ .

For wavelengths of the order of those used in telecommunications  $\lambda_1 \simeq 1.55\mu\text{m}$ , the attenuation of 0.15 db per kilometer (see eq.(16)) corresponds to a dimensionless attenuation parameter,  $\text{Im } \delta$ , of the order of

$$\text{Im } \delta = -\frac{1.55\mu\text{m}}{4\pi 10^9\mu\text{m}} \ln 0,966 \simeq 4.3 \times 10^{-12} \quad (47)$$

It is then clear from fig.(4) that orders of approximately  $\mathcal{N} \simeq 10$  are called for in order to obtain comparable attenuations.

## 2.2. Field map

One can remark that the mode propagation constants are calculated entirely in terms of impedances, and that it was not necessary to obtain explicitly the field configuration in order to identify a mode. Nevertheless, the field configuration can prove useful in obtaining a physical understanding of the

guided modes. We recall that the electric field for TE waves in layer  $j$  and its square amplitude are given by

$$\mathcal{E}^{(j)}(x, y) = (a_j^- e^{-i\alpha_j \bar{y}} + a_j^+ e^{i\alpha_j \bar{y}}) e^{i\gamma x} \mathbf{e}_z \quad (48)$$

so that

$$\begin{aligned} \left| \mathcal{E}^{(j)}(x, y) \right|^2 &= e^{-2x \operatorname{Im} \gamma} \\ &\cdot \left( |a_j^-|^2 e^{2\bar{y} \operatorname{Im} \alpha_j} + |a_j^+|^2 e^{-2\bar{y} \operatorname{Im} \alpha_j} + 2 \operatorname{Re} \{ a_j^+ a_j^{-,*} e^{i2\bar{y} \operatorname{Re} \alpha_j} \} \right). \end{aligned} \quad (49)$$

Therefore, a description of the field configuration requires the knowledge of the field coefficients.

Expressing the fields  $\mathcal{E}_z^{(j)}$  and  $\mathcal{H}_x^{(j)}$  in terms of  $a_j^+$  and  $a_j^-$ , one obtains from the definition of  $Z_{\text{en}}^{(j-1)}$ , eq.(15), a relation between  $a_j^+$  and  $a_j^-$  :

$$a_j^+ = a_j^- \frac{Z_{\text{en}}^{(j-1)} + Z_j}{Z_{\text{en}}^{(j-1)} - Z_j} e^{-2i\alpha_j \bar{y}_{j-1}} \quad \forall j \in [2, N] \quad (50)$$

The  $a_j^-$  are readily determined using a recurrence relation. Continuity of the tangential electric field at the interfaces implies that

$$a_{j-1}^- e^{-i\alpha_{j-1} \bar{y}_{j-1}} + a_{j-1}^+ e^{i\alpha_{j-1} \bar{y}_{j-1}} = a_j^- e^{-i\alpha_j \bar{y}_{j-1}} + a_j^+ e^{i\alpha_j \bar{y}_{j-1}} \quad \forall j \in [1, N] \quad (51)$$

For the  $j = 1$  interface, a propagating mode implies that  $a_1^- = 0$  and this relation together with eq.(50) yields

$$a_1^+ e^{i\alpha_1 \bar{y}_1} = a_2^- e^{-i\alpha_2 \bar{y}_1} + a_2^- \frac{Z_{\text{en}}^{(1)} + Z_2}{Z_{\text{en}}^{(1)} - Z_2} e^{-2i\alpha_2 \bar{y}_1} e^{i\alpha_2 \bar{y}_1}$$

*i.e.*

$$a_2^- = \frac{Z_{\text{en}}^{(1)} - Z_2}{2Z_{\text{en}}^{(1)}} e^{i(\alpha_1 + \alpha_2) \bar{y}_1} a_1^+ \quad (52)$$

Invoking the mode condition ( $Z_{\text{en}}^{(1)} = Z_1$ ) we then obtain :

$$\begin{aligned} a_2^- &= \frac{Z_1 - Z_2}{2Z_1} e^{i(\alpha_1 + \alpha_2) \bar{y}_1} a_1^+ \\ a_2^+ &= \frac{Z_1 + Z_2}{2Z_1} e^{i(\alpha_1 - \alpha_2) \bar{y}_1} a_1^+ \end{aligned} \quad (53)$$

The coefficients of the other layers may be determined by compact recursive formulae invoking the impedances

$$\begin{aligned} a_{j-1}^- &= \frac{Z_{\text{en}}^{(j-1)} - Z_{j-1}}{Z_{\text{en}}^{(j-1)} - Z_j} a_j^- e^{i(\alpha_{j-1} - \alpha_j) \bar{y}_{j-1}} & \forall j \in [3, N+1] \quad (54) \\ a_j^+ &= a_{j-1}^+ \frac{Z_{\text{en}}^{(j-1)} + Z_j}{Z_{j-1} + Z_{\text{en}}^{(j-1)}} e^{i(\alpha_{j-1} - \alpha_j) \bar{y}_{j-1}} & \forall j \in [3, N+1] \end{aligned}$$

These relations can either both be applied, or one can apply only one of them, and obtain the other via eq.(50). The overall normalization of the coefficients is arbitrary, and we chose to fix it by setting the amplitude of the downward going coefficient of the central layer to unity,  $|a_c^-| = 1$ , where the index  $c$  denotes the central layer,  $c \equiv 2N + 1$ .

One may object to the fact that the recurrence relations in eq.(54) appear susceptible to numerical instabilities should the denominator prove to be zero. In practice, this does not generally appear to pose a problem. Should a near division by zero arise however, the problem may be avoided by defining

$$a_j^- \equiv \left( Z_{\text{en}}^{(j-1)} - Z_j \right) \tau_j. \quad (55)$$

With this definition, we conclude

$$\tau_2 = \frac{e^{i(\alpha_1 + \alpha_2) \bar{y}_1}}{2Z_1} a_1^+ \quad (56)$$

while the  $a_j^-$  recurrence relation of eq.(54) then takes the form

$$\tau_{j+1} = \frac{Z_{\text{en}}^{(j-1)} - Z_j}{Z_{\text{en}}^{(j)} - Z^{(j)}} e^{i(\alpha_{j+1} - \alpha_j) \bar{y}_j} \tau_j \quad \forall j \in [2, N]. \quad (57)$$

Invoking the relation

$$\frac{Z_{\text{en}}^{(j-1)} - Z^{(j)}}{Z_{\text{en}}^{(j)} - Z^{(j)}} = \frac{1 + i \tan \psi_j}{1 - \frac{Z_{\text{en}}^{(j)}}{Z_j} i \tan \psi_j} \quad j \in [2, N] \quad (58)$$

the recurrence relation for the  $\tau_j$  coefficients can be determined recursively

$$\tau_{j+1} = \left\{ \frac{1 + i \tan \psi_j}{1 - \frac{Z_{\text{en}}^{(j)}}{Z_j} i \tan \psi_j} \right\} e^{i(\alpha_{j+1} - \alpha_j) \bar{y}_j} \tau_j \quad \forall j \in [2, N] \quad (59)$$

starting from eq.(56) as the initialization.

### 2.3. Dispersion relations

In waveguide theory, it is natural to interest ourselves in the properties of the modes, and most notably the dispersion relations. In this work, our goal is not to describe all possible modes, and we content ourselves with describing the principal leaky mode of propagation for which the field is trapped inside the central layer. Consequently, we adopt techniques requiring an approximate starting solution. For fibers optimally designed as in section (2.2.1), and operating at the optimal frequency,  $\omega_{\text{op}}$ , an excellent approximate solution is given by  $\delta = \delta_{\text{op}} + i\delta''$  where  $\delta''$  is given by eq.(44). The dispersion properties of the mode can then be determined by making small incremental steps in frequency, and obtain the new solutions of  $\delta$  at each frequency.

As in section (2.2.1) where we discussed the design of infinite fibers, we found that the numerical sensitivity to the properties of the central layer is such that it is preferable to solve for  $\delta$  in terms via conditions imposed on the interfaces of the central layer. One proceeds by calculating  $Z_{\text{en}}^{(2\mathcal{N}+2)}$  and  $Z_{\text{en}}^{(2\mathcal{N}+1)}$  via the ascending and descending recurrence relations, eqs.(16) and (20) respectively, using an approximate value for  $\delta$ . Thus,  $Z_{\text{en}}^{(2\mathcal{N}+2)}$  and  $Z_{\text{en}}^{(2\mathcal{N}+1)}$  are functions of the approximate value of  $\delta$  via the region impedances and the  $\psi_j$  for the bi-layers. The  $\psi_j$  for the crystal layers can be reexpressed

$$\psi_j \equiv \alpha_j (\bar{y}_j - \bar{y}_{j-1}) \equiv \sqrt{\frac{\bar{n}_j^2 - \delta^2}{\bar{n}_j^2 - \delta_{\text{op}}^2}} \frac{\lambda_1^{\text{op}}}{\lambda} \sqrt{\bar{n}_j^2 - \delta_{\text{op}}^2} \frac{2\pi}{\lambda_1^{\text{op}}} (y_j - y_{j-1}) \quad (60)$$

which simplifies using the relations satisfied by  $\delta_{\text{op}}$ , namely

$$\begin{aligned} \sqrt{\bar{n}_h^2 - \delta_{\text{op}}^2} \frac{2\pi}{\lambda_1^{\text{op}}} \Delta y_h &= -\frac{\pi}{2} \\ \sqrt{\bar{n}_b^2 - \delta_{\text{op}}^2} \frac{2\pi}{\lambda_1^{\text{op}}} \Delta y_b &= -\frac{\pi}{2} \end{aligned} \quad (61)$$

The  $\psi_j$  for high and low index materials  $\psi_h$  and  $\psi_b$  respectively then take the form

$$\begin{aligned} \psi_h &= -\sqrt{\frac{\bar{n}_h^2 - \delta^2}{\bar{n}_h^2 - \delta_{\text{op}}^2}} \frac{\lambda_1^{\text{op}}}{\lambda} \frac{\pi}{2} \\ \psi_b &= -\sqrt{\frac{\bar{n}_b^2 - \delta^2}{\bar{n}_b^2 - \delta_{\text{op}}^2}} \frac{\lambda_1^{\text{op}}}{\lambda} \frac{\pi}{2} \end{aligned} \quad (62)$$

The phase variable of the central layer,  $\psi_c$ , for an  $m$  order propagating mode

must then satisfy

$$\psi_c \equiv \psi_{2\mathcal{N}+1} = \tan^{-1} \left[ i Z_c \frac{Z_{\text{en}}^{(2\mathcal{N})} - Z_{\text{en}}^{(2\mathcal{N}+1)}}{Z_c^2 - Z_{\text{en}}^{(2\mathcal{N})} Z_{\text{en}}^{(2\mathcal{N}+1)}} \right] - m\pi \equiv \Lambda(m, \delta, \lambda) \quad (63)$$

Using the definition of  $\psi_c$  (eq.(17)), eq.(63) can be rewritten

$$\psi_c \equiv \alpha_{2\mathcal{N}+1} (\bar{y}_{2\mathcal{N}+1} - \bar{y}_{2\mathcal{N}}) = -\sqrt{\frac{\bar{n}_c^2 - (\delta' + i\delta'')^2}{\bar{n}_c^2 - \delta_{\text{op}}^2}} \sqrt{\bar{n}_c^2 - \delta_{\text{op}}^2} \Delta y_c \frac{2\pi}{\lambda_1^{\text{op}}} \left( \frac{\lambda_1^{\text{op}}}{\lambda} \right) = \Lambda \quad (64)$$

Recalling that  $\delta_{\text{op}}$ , and  $\Delta y_c$  satisfy the relation

$$\sqrt{\bar{n}_c^2 - \delta_{\text{op}}^2} \Delta y_c \frac{2\pi}{\lambda_1^{\text{op}}} = -m_{\text{op}}\pi \quad (65)$$

the propagation constant of the mode,  $\delta$ , must thus satisfy

$$\sqrt{\frac{\bar{n}_c^2 - (\delta' + i\delta'')^2}{\bar{n}_c^2 - \delta_{\text{op}}^2}} \left( \frac{\lambda_1^{\text{op}}}{\lambda} \right) = -\frac{\text{Re } \Lambda}{m_{\text{op}}\pi} - i \frac{\text{Im } \Lambda}{m_{\text{op}}\pi} \quad (66)$$

from which we obtain two coupled equations for  $\delta'$  and  $\delta''$ .

$$\begin{aligned} \delta' &= \sqrt{\bar{n}_c^2 - \lambda^2 (\bar{n}_c^2 - \delta_{\text{op}}^2) \frac{(\text{Re } \Lambda)^2 - (\text{Im } \Lambda)^2}{m_{\text{op}}^2 \pi^2 (\lambda_1^{\text{op}})^2} - (\delta'')^2} \\ \delta'' &= -\frac{\lambda^2 (\bar{n}_c^2 - \delta_{\text{op}}^2) (\text{Re } \Lambda)(\text{Im } \Lambda)}{m_{\text{op}}^2 \pi^2 (\lambda_1^{\text{op}})^2 \delta'} \end{aligned} \quad (67)$$

The value of  $\delta$  gives a new estimation for the solution. One must recall however that  $\Lambda$  is itself a function of  $\delta$ . These solutions must therefore be solved self-consistently. Although simple iteration is often sufficient to find self-consistent solutions, it is generally more efficient to use more sophisticated techniques like those employing homographic approximations.[11] The approximate solutions given by the optimal solutions generally provide sufficiently good starting values for iterative or homographic techniques.

We now show the dispersion relations for TE modes calculated using our technique. The physical media are chosen to be the same as for previous examples,  $\bar{n}_b = \bar{n}_c = 1$ ,  $\bar{n}_h = 1.95$ ,  $\mu_1 = \mu_b = \mu_c = \mu_h = 1$ . The thickness of the central gap was chosen such that only the lowest mode,  $m_{\text{op}} = 1$  exists at the optimum frequency. In fig.5a), we illustrate the real part of the dispersion relations for the principal guided modes in a fiber designed for  $\delta_{\text{op}} = 0.7$ . Specifically, we plot  $\omega/\omega_{\text{op}} \text{Re } \delta$  of the propagating modes as a function of  $\omega/\omega_{\text{op}}$ . We have

multiplied the dimensionless factor  $\delta$  by  $\omega/\omega_{\text{op}}$  so that if we invert the graph such that  $\omega$  is a function of  $\delta$  then the position of a point will correspond to the phase velocity of the mode on a scale normalized such that  $c = 1$ . The slope of the tangent of the inverted graph then yields the group velocity of the mode. It is interesting to remark in fig.(5) that the low lying modes apparently begin with a zero group velocity.

One can also observe in fig.5a) that the  $m = 1$  guided mode continues to exist for a relatively large frequency range around  $\omega_{\text{op}}$ . We abruptly cease to find a solution however below a lower limit  $\omega_{\text{min}}$ . Our technique also abruptly ceases to obtain solutions above a maximum frequency  $\omega_{\text{max}}$ . At about this same frequency however, we begin to find  $m = 3$  guided mode solutions. This behavior repeats itself for higher frequencies, and we have plotted the modes up through the  $m = 9$  solutions. It is interesting to note that the range of frequencies for each mode is approximately the same. We did not find modes where  $m$  is even since we designed the fiber to confine modes where  $m$  is odd. Consequently, the photonic band gap effect no longer operates in the neighborhoods even multiples of  $\omega_{\text{op}}$  where even modes would be expected to exist. This situation would have been inverted had we designed the fiber to confine even modes.

In order for a leaky mode to be useful for guiding waves over a long distance, their imaginary parts must be quite small. In order to evaluate this effect, we plot in fig.5b) the  $\log_{10}$  of the imaginary parts of the dispersion relations for the same frequencies as in fig.5a). Although we can easily remark that  $\text{Im } \delta$  are smallest for the  $m = 1$  mode for which the fiber is designed, the imaginary parts of higher modes can still be quite small, and these modes may prove useful. From this figure, it is clear for all modes that  $\text{Im } \delta$  becomes rather large near the edges of the propagating band, and consequently that the usefulness of the modes is compromised for frequencies too far from the centers of the propagating bands. We remark that, as expected, the minima of  $\text{Im } \delta$  occur at frequencies near  $\omega_{\text{op}}$ ,  $3\omega_{\text{op}}$ ,  $5\omega_{\text{op}}$ , *etc.* Apparently, the fact that these minima do not occur precisely at odd multiples of  $\omega_{\text{op}}$ , cannot be regarded as a consequence of the finite number of multilayers. Instead, this should be viewed as a consequence that our fiber design procedure does not guarantee a minimum of the attenuation at this point.

The physical behavior of the modes in different regions of the dispersion curves may be better understood by looking at field amplitude plots of the modes at different frequencies. In figure 6, we illustrate the square amplitude of the electric field plotted with respect to the  $y$  coordinates for four frequencies on the  $m = 1$  dispersion curve. The outer edges of the 1-D fiber walls are placed at  $y = \pm 1$  respectively. In fig.6a) is the field map for mode  $m = 1$  at  $\omega = \omega_{\text{op}}$ . In fig.6b) is the field map at the minimum of  $\text{Im } \delta$ ,  $\omega \simeq 1.51 \omega_{\text{op}}$ . One observes that mode in 6b) does indeed appear more tightly confined than the mode at the design frequency, 6a). We remark that both modes are largely confined to

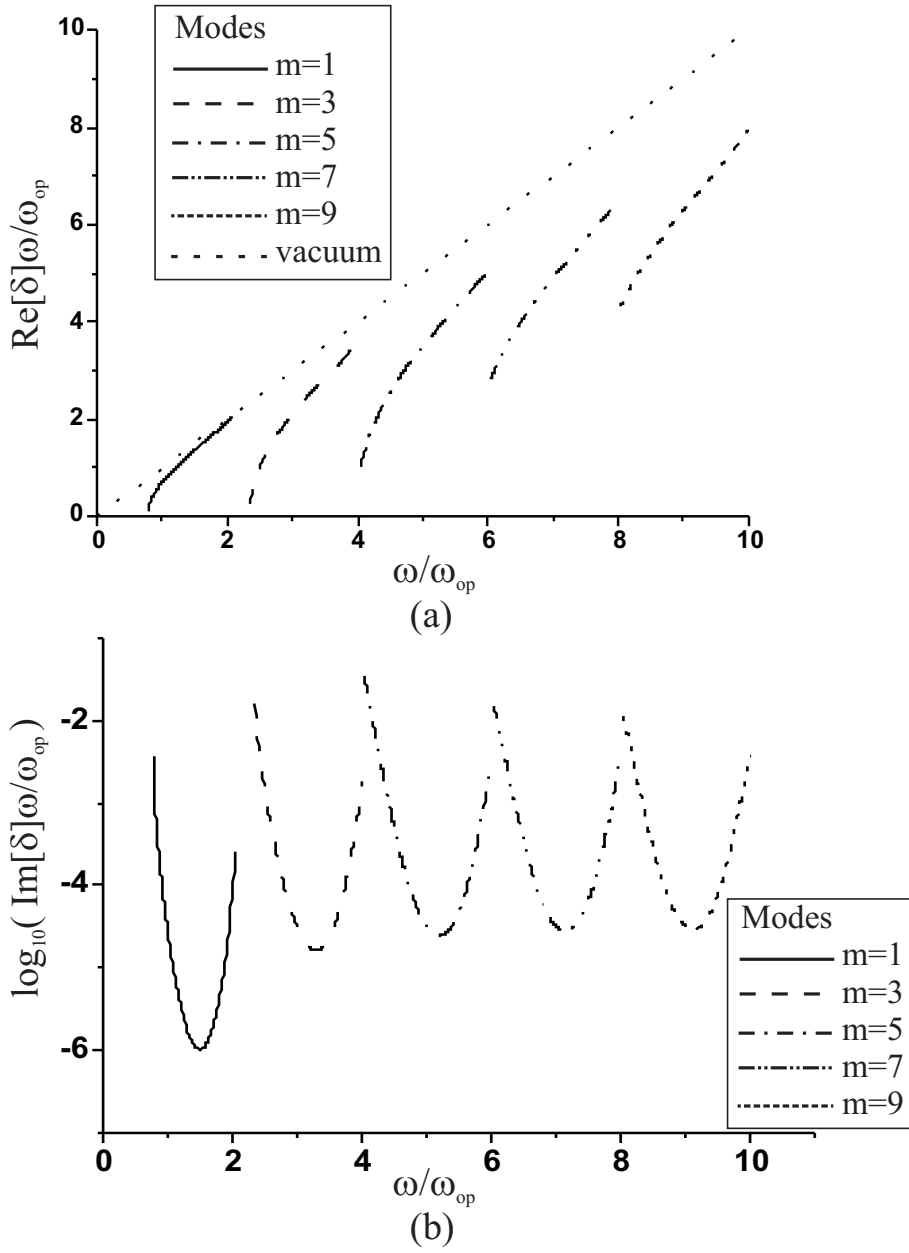


FIG. 5: Dispersion relations for propagation along the fiber axis, *i.e.*  $\gamma$  vs.  $\omega$ , for modes in a 1-D PBF “optimized” for  $\delta_{op} = 0.7$ ,  $m_{op} = 1$ , ( $\Delta y_h \simeq 0.137\lambda_1^{op}$ ,  $\Delta y_b \simeq 0.35\lambda_1^{op}$ ,  $\Delta y_c \simeq 0.7\lambda_1^{op}$ ). a) Illustrates the real part of the dispersion relation. b) Illustrates the imaginary part. There are 5 high index layers on each side of the central layer,  $\mathcal{N} = 5$

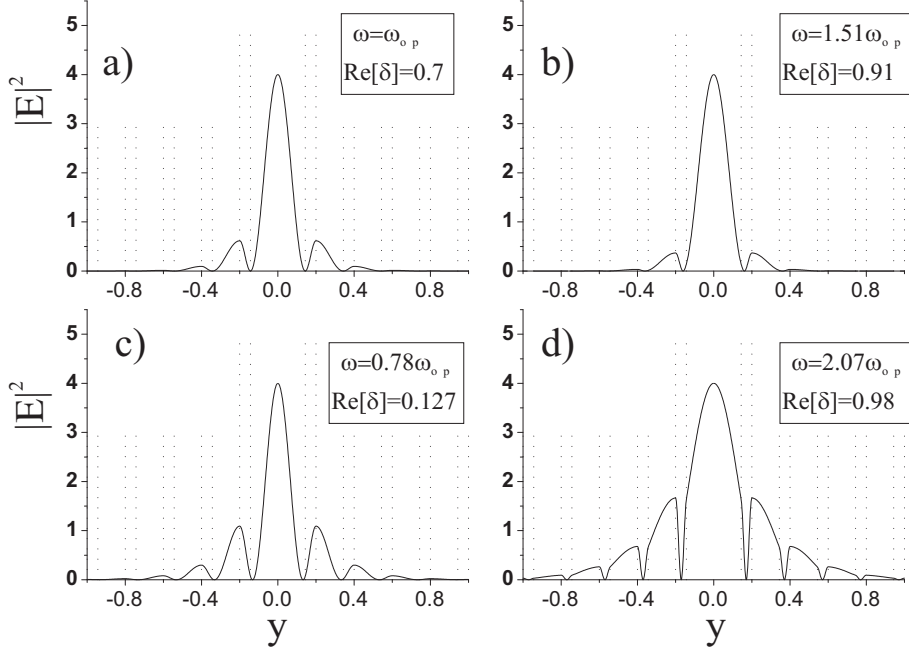


FIG. 6: Squared field amplitudes,  $|\mathcal{E}^{(j)}(y)|^2$  in arbitrary units for the  $m = 1$  modes in a 1-D PBF “optimized” for  $\delta_{\text{op}} = 0.7 m_{\text{op}} = 1$ , ( $\Delta y_h \simeq 0.137\lambda_1^{\text{op}}$ ,  $\Delta y_b \simeq 0.35\lambda_1^{\text{op}}$ ,  $\Delta y_c \simeq 0.7\lambda_1^{\text{op}}$ ). Dashed lines show the location of the interfaces.

the central layer despite our quite small number of bi-layers,  $\mathcal{N} = 5$ . It is also worth remarking that the field found outside the central layer is predominately located within vacuum layers. In figures 6c) and 6d), are illustrated the field maps at the lower and upper edges of the  $m = 1$  propagating band,  $\omega \simeq 0.78\omega_{\text{op}}$  and  $\omega \simeq 2.07\omega_{\text{op}}$  respectively. At the lower edge of the propagating band, fig.6c), one can see that the field has spread out somewhat into the crystalline walls compared to modes near  $\omega_{\text{op}}$ . At the upper edge of the propagating band however, fig.6d), the field has spread considerably further into the entire width of crystalline walls. In view of this field map, it is not too surprising that the propagation constant has a small but non-negligible imaginary part  $\frac{\omega}{\omega_{\text{op}}} \text{Im} \delta \simeq 0.00012$  at this frequency. We nevertheless remark that the field continues to avoid somewhat the interior of the high index layers.

It is of interest to study the mode characteristics for a higher number of bi-layers. In fig.7, we calculate the same dispersion relations as in fig.5 for PBF

containing now  $\mathcal{N} = 15$  high index layers on each side of the central layer, (as opposed to  $\mathcal{N} = 5$  in fig.5). When compared to the  $\mathcal{N} = 5$  model, we see that the principal effect on  $\text{Re } \delta$  is to open up the stop bands between different propagating modes. As expected, the  $\text{Im } \delta$  is here considerably lowered with respect to the  $\mathcal{N} = 5$  model. Analogously to the  $\mathcal{N} = 5$  model, the minimum of  $\text{Im } \delta$  is somewhat shifted from odd multiples of  $\omega_{\text{op}}$ . One can guess that, from the small imaginary parts of the mode even at the band edges, the modes remained well confined in this case even at the edge of each propagating band. Field maps of the modes, not shown here, readily confirm this point. It is interesting that the disappearance of a leaky mode is not simply due to a gradual inability of the crystal to confine the wave, but ceases suddenly in a region where the mode is still well confined.

#### 2.4. Absorption in photonic crystal fibers

The previous paragraphs treated PBFs composed of a lossless high index material and a lossless vacuum. Should we add a realistic absorption to the high index material, the results imply that the absorption of a PBF mode should be less than the absorption in a classical high index fiber. This conjecture can be put to the test by explicit mode calculations. This is done by taking the same procedure as for obtaining the dispersion relations in the preceding paragraph, but now leaving the frequency fixed and adding an imaginary part to the high index material. In fig.8 we illustrate a log-log plot of the attenuation in an  $m = 1$  mode in a  $\mathcal{N} = 15$  fiber having the same thicknesses as in fig.7 as a function of  $\text{Im } n_h$ . The frequency demonstrating minimal attenuation for this fiber,  $\omega \simeq 1,49\omega_{\text{op}}$ , was chosen.

We would like to compare these attenuations to those obtained for a classic high index waveguide. However, it is not immediately clear what characteristics should be chosen to make a meaningful comparison. Nevertheless, we can expect the attenuation of a classic high index waveguide to be of the same order of magnitude as the attenuation in the bulk high index medium. Therefore, we also plot the attenuation for a bulk high index material. As can be seen from the graph, the attenuation in the fiber waveguide has been substantially reduced from that of the bulk high index material,  $\frac{\delta''_{\text{bulk}}}{\delta''_{\text{fiber}}} \simeq 20$ . This result suggests that compared to classic fibers, order of magnitude decreases in absorption of PBFs are feasible.

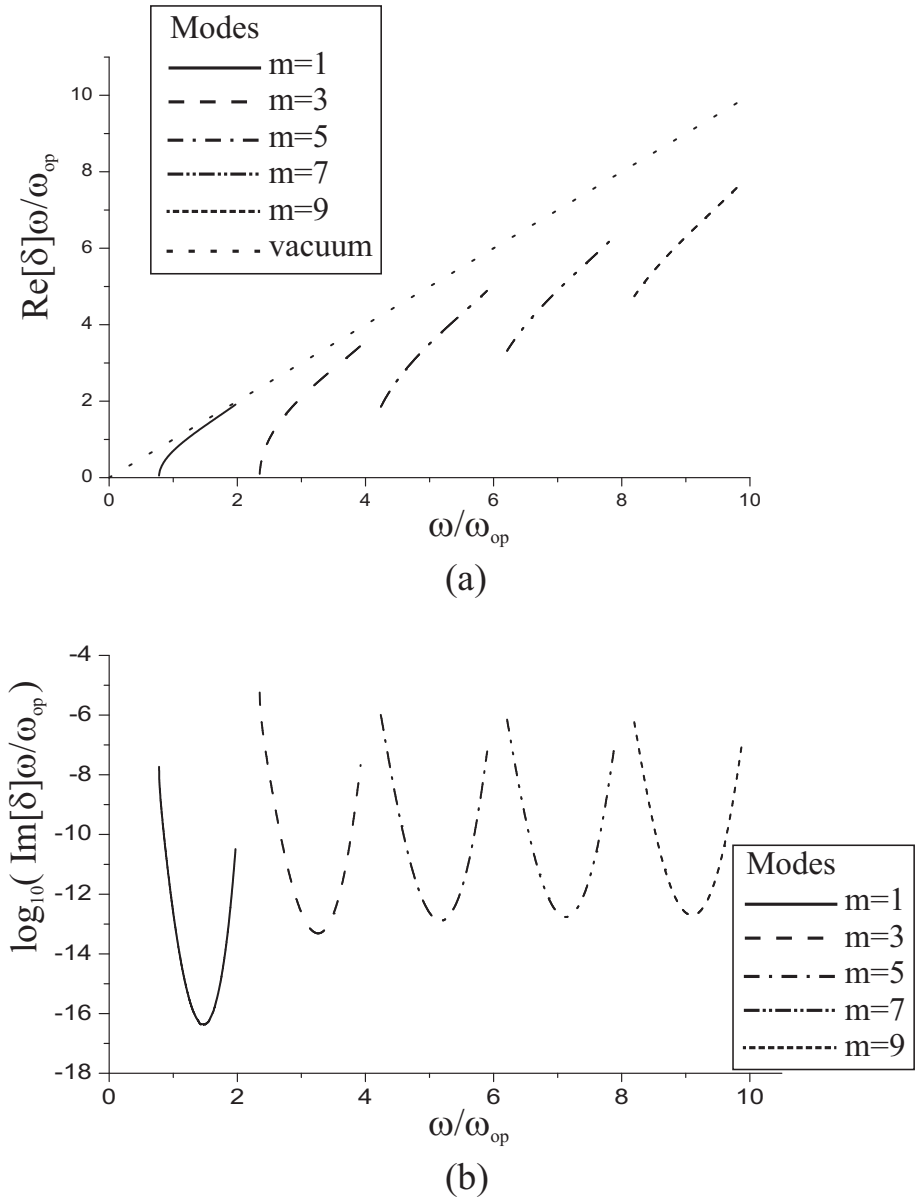


FIG. 7: Dispersion relations for propagation along the fiber axis, with the same parameters as in Fig.5, except that the number of Bragg layers has been enlarged to 15 high index layers on each side of the central layer,  $\mathcal{N} = 15$ .

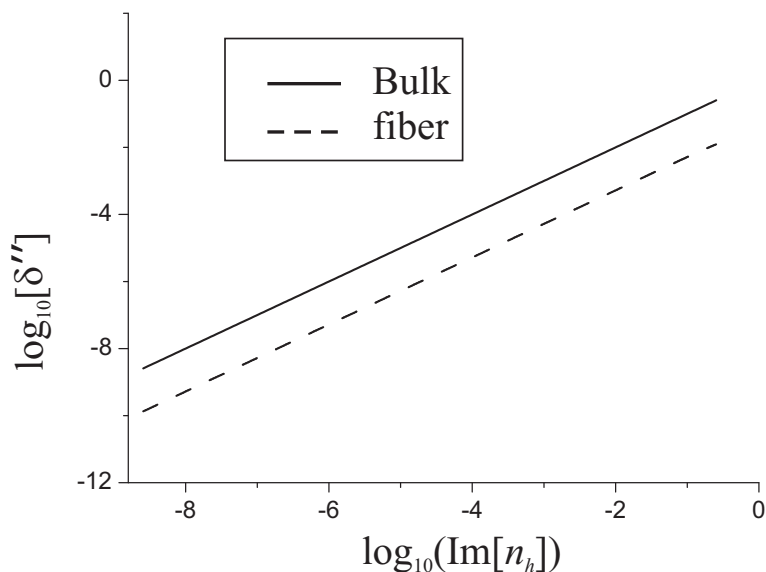


FIG. 8: Attenuation,  $\delta''$  in a vacuum to high index PBF as a function of  $\text{Im } n_h$  added to the real dielectric constant,  $\text{Re } \varepsilon = 1.95^2$ . Attenuation for propagation in a bulk material of index  $n_h$  is shown for comparison. The PBF is optimized for  $\delta_{\text{op}} = 0.7$ ,  $m_{\text{op}} = 1$ , ( $\Delta y_h \simeq 0.137\lambda_1^{\text{op}}$ ,  $\Delta y_b \simeq 0.35\lambda_1^{\text{op}}$ ,  $\Delta y_c \simeq 0.7\lambda_1^{\text{op}}$ ).

### 3. CONCLUSION

Our calculations indicate that low index core PBFs can probably be designed to be essentially monomode for TE waves over a relatively large range of frequencies. We have also illustrated that absorptive losses can be considerably reduced for such fibers. We have demonstrated that the impedance formulation can be used to good effect in this problem. Despite the efficiency of the numerical method, we found that the numeric behavior of the solutions for such fibers are extremely sensitive to the properties of the central “defect” layer. Consequently, we were obliged to treat this layer separately from the rest in order to obtain reliable numeric results. Further work concerning the physical significance of the leaky modes should be carried out. We have not at all ruled out the possibility of the existence of additional leaky modes, nor addressed the possibility of the coupling of our leaky modes with additional modes. In a forthcoming paper, we look at TM modes in such fibers, and the possibilities for the coexistence of TE and TM modes.

## References

---

- [1] Knight J.C., Birks T.A., Cregan R.F., Russell P.S.J., de Sandro J.P., "Photonic crystals as optical fibres - physics and applications", *Opt. Mater.* 11, 143-151, 1999.
- [2] Barkou S.E., Broeng J., Bjarklev A., "Silica-air photonic crystal fiber design that permits waveguiding by a true photonic bandgap effect", *Opt. Lett.* 24, 46-48, 1999.
- [3] Ferrando A., Silvestre E., Miret J.J., Andres P., "Full-vector analysis of a realistic photonic crystal fiber", *Opt. Lett.* 24, 276-278, 1999.
- [4] Monro T.M., Richardson D.J., Broderick N.G.R., Bennett P.J., "Holey optical fibers: An efficient modal model", *J. Lightwave Technol.* 17, 1093-1102, 1999.
- [5] Mogilevtsev D., Birks T.A., Russell P.S., "Group-velocity dispersion in photonic crystal fibers", *Opt. Lett.* 23, 1662-1664, 1998.
- [6] K.M. Lo, R.C. McPhedran, I.M. Basserr, and G.W. Milton, "An Electromagnetic Theory of Dielectric Waveguides With Multiple Embedded Cylinders", *Journal of Lightwave Technology*, Vol. 12 No. 3, 1994.
- [7] E. Yablonovitch. "Inhibited spontaneous emission in solid-state physics and electronics", *Phys.Rev.Lett.* Vol. 58, 2059-2062, 1987.
- [8] J.D. Joannopoulos, et al., *Photonic Crystals : Molding the Flow of Light*, Princeton U. Press, Princeton NJ, 1995.
- [9] A.K. Cousins and S.C. Gottschalk, "Applications of the Impedance Formalism to Diffraction Gratings with Multiple Coating Layers", *Appl. Opt.* 29, 4268, 1990.
- [10] M.Nevière, "The Homogenous Problem", in *Topics in Current Physics*, Vol. 22 *Electromagnetic Theory of Gratings*, Springer-Verlag, Berlin Heidelberg, 1980.
- [11] M.Nevière, P.Vincent,R.Petit, and M.Cadilhac "Systematic Study of Resonances of Holographic Thin Film Couplers", *Optics Comm.* Vol. 9 No.1 48, 1973.